

This is an Open Access document downloaded from ORCA, Cardiff University's institutional repository: <https://orca.cardiff.ac.uk/id/eprint/98123/>

This is the author's version of a work that was submitted to / accepted for publication.

Citation for final published version:

Lupan, Oleg, Postica, Vasile, Gröttrup, Jorit, Mishra, Abhishek K., De Leeuw, Nora and Adelung, Rainer 2017. Enhanced UV and ethanol vapour sensing of a single 3-D ZnO tetrapod alloyed with Fe₂O₃ nanoparticles. *Sensors and Actuators B: Chemical* 245 , pp. 448-461. 10.1016/j.snb.2017.01.107

Publishers page: <http://dx.doi.org/10.1016/j.snb.2017.01.107>

Please note:

Changes made as a result of publishing processes such as copy-editing, formatting and page numbers may not be reflected in this version. For the definitive version of this publication, please refer to the published source. You are advised to consult the publisher's version if you wish to cite this paper.

This version is being made available in accordance with publisher policies. See <http://orca.cf.ac.uk/policies.html> for usage policies. Copyright and moral rights for publications made available in ORCA are retained by the copyright holders.



Enhanced UV and ethanol vapour sensing of a single 3-D ZnO tetrapod alloyed with Fe₂O₃ nanoparticles

Oleg Lupan^{a,b,*}, Vasile Postica^b, Jorit Gröttrup^a, Abhishek K. Mishra^{c,d}, Nora H. de Leeuw^e, Rainer Adelung^{a,*}

^a Functional Nanomaterials, Faculty of Engineering, Institute for Materials Science, Kiel University, Kaiser Str. 2, D-24143, Kiel, Germany

^b Department of Microelectronics and Biomedical Engineering, Technical University of Moldova, 168 Stefan cel Mare Av., MD-2004, Chisinau, Republic of Moldova

^c Department of Chemistry, University College London, 20 Gordon Street, London WC1H 0AJ, UK

^d Research & Development, University of Petroleum and Energy Studies (UPES), Bidholi, Dehradun 248007, India ^e School of Chemistry, Cardiff University, Main Building, Park Place, Cardiff, CF10 3AT, UK

Abstract

Fabrication of multifunctional devices based on nano- and microstructures of a single semiconducting oxide is an important step for a better understanding of their maximum sensing properties and the base for the development of bottom-up nanotechnologies. In this work we have fabricated, for the first time devices based on a single or two interconnected ZnO tetrapods (T), doped with Fe and alloyed with Fe₂O₃ nanoparticles (NPs) and microparticles (MPs) in order to improve their sensing properties towards ultraviolet (UV) sensing and ethanol vapour (EtOH). Compared to pristine ZnO-T improved UV and gas sensing properties of Fe-doped ZnO-T were observed. By Fe₂O₃-alloying of Fe-doped ZnO-T further improvement in sensing properties was obtained with a reduced influence of the relative humidity (RH) on the sensing response. A gas sensing mechanism was proposed and discussed in detail based on the alloyed Fe₂O₃ NPs and MPs. The results presented here demonstrate the efficiency of doping and alloying of single ZnO microstructures with other semiconducting oxides to improve their sensing properties, including the decrease in influence of RH on the gas response and the rapidity of the sensors.

Keywords:

Single tetrapod
Zinc oxide
Hetero
Ethanol
Nanosensor
Hybrid

1. Introduction

It is well known that the main disadvantage of micro- and nanostructures of pure semiconducting oxides, such as SnO₂ and ZnO, is their low selectivity and poor stability to environments with a high relative humidity (RH) [1–3]. Thus, a variety of methods has been elaborated for an improvement of gas sensors based on semiconducting oxides, including the synthesis of different morphologies [4], doping [5], surface functionalization with noble metals [6], polymers [7] and other semiconducting oxides for the formation of nanoscale hetero-junctions or core-shell structures [8]. Many of these methods combine important disadvantages such as additional technological steps, poor long-time stability and repeatability, with advantages such as improved selectivity, sensi-

tivity and stability to high RH. The main mechanism responsible for these improvement is the electronic and chemical sensitization of the micro- and nanostructures, which results in different modifications of electrical and chemical properties, including modulation of the conduction channel, Debye length (D) and others [6,9].

For example, Zhu et al. demonstrated enhanced ethanol sensing performances of -Fe₂O₃/ZnO hetero-structures which were attributed to a smaller thickness of the ZnO shell resulting in a higher modulation of the conduction channel under exposure to ethanol [10]. Si et al. also demonstrated an improved ethanol gas response for Fe₂O₃/ZnO core/shell nano-rods with an excellent long-term stability, which is very attractive for practical applications [11]. Huang et al. fabricated highly selective ethanol sensors based on ZnO/-Fe₂O₃ hierarchical nano-structures with a high rapidity at an operating temperature of 370 °C and excellent long-term stability. The highest gas response was obtained at an optimal content of -Fe₂O₃ at 2% [12]. Another interesting gas sensing application was reported by Zhu et al. demonstrating the highly

* Corresponding authors.

E-mail addresses: ollu@tf.uni-kiel.de, oleg.lupan@mib.utm.md (O. Lupan), ra@tf.uni-kiel.de (R. Adelung).

sensitive detection of ethanol at room temperature by $\text{Fe}_2\text{O}_3/\text{ZnO}$ nanowire piezo-nanogenerator as self-powered gas sensor [13].

It has also been demonstrated that a combination of Fe_2O_3 structures with other types of metal oxides is a very efficient method to enhance the ethanol vapour response and selectivity. Suryawan-shi et al. modified the surface of thick Cr_2O_3 films with Fe_2O_3 which allows to selectively detect different reducing gases at different operating temperatures, including ethanol at an operating temperature of 300°C [14]. Furthermore, Kim et al. demonstrated enhanced ethanol response of In_2O_3 nanowires (NWs) functionalized with Fe_2O_3 NPs [15], whereas Choi et al. coated SnO_2 NWs with Fe_2O_3 NPs to greatly enhance ethanol sensing performances which they attributed to an increase in grain boundaries, i.e. more potential energy barriers [16]. All these results can be also attributed to the fact that Fe_2O_3 is known to be a good catalyst for volatile organic compounds (VOCs) and can essentially improve gas sensing properties for detection of VOCs [17,18]. However, no results have been reported to date on UV sensing properties of ZnO micro- and nano-structures modified/functionalized with Fe_2O_3 , although the $\text{Fe}_2\text{O}_3/\text{ZnO}$ interface is known to be a very effective hole-electron separator and can reduce the electron-hole recombination probability, which was demonstrated in photocatalytic applications [19].

Due to the rapid progress in nanotechnologies, the next significant step in UV and gas sensing applications was the fabrication of nanosensors, i.e. devices based on a single semiconducting oxide micro- or nanostructure [9,20], as well as individual ZnO tetrapods. For example, Zheng et al. fabricated a multi-terminal oxygen sensor based on an individual ZnO tetrapod [21], whereas Zhang et al. designed a multiterminal sensor using an individual ZnO tetrapod which was capable of detecting light with different wavelengths and distinguishing false responses [22]. Due to a high surface-to-volume ratio, such devices can detect very low concentrations (sub ppm) of gaseous and biological species at room temperature [9,23], thus excluding the necessity to fabricate micro-heaters and essentially reducing the power consumption and fabrication cost [24]. Furthermore, due to the high resistivity of the micro- and nanostructures of semiconducting oxides, an ultra-low power consumption is possible [25] which is important for long-term applications. The main advantage of such nanodevices is the efficient way of controlling the electrical and chemical properties of single micro- and nanostructures [9]. For example, the formation of a Schottky contact at one end of a ZnO NW introduces an essential enhancement in the sensing properties [23], due to the high sensitivity of the Schottky barrier height on UV illumination, gaseous and chemical species which can change the local electric-field distribution [23]. Thus, nanodevices have attracted significant attention due to their extensive applications and the possibility of their integration into mobile applications, smart devices, etc. As a result, many investigations have been performed in the area of nanodevice fabrication, especially for UV and gas sensing applications [1,9,20,23] and the already enumerated methods to improve the properties of gas sensors have been applied to nanodevices [7,9]. For example, Lao et al. functionalized a single ZnO nanobelt with polymers that has a high UV absorption ability leading to an enhancement of the UV response by close to 5 orders of magnitude [7]. Kuang et al. demonstrated that additional heterojunctions formed at the surfaces of individual structures of metal oxides play a critical role in controlling the charge transport through the structure, i.e. device sensitivity [26].

However, to the best of our knowledge of the scientific literature, to date the UV and gas sensing properties of hybridized tetrapod structures of single three-dimensional (3D) semiconducting oxides alloyed with other semiconducting oxide NPs and MPs have not been reported. In previous work, our group has demonstrated that hybridized ZnO tetrapod (T) networks possess enhanced sensing properties compared to pristine ZnO -T networks [27]. For a better

understanding of the sensing properties it is therefore interesting to investigate the influence of oxide microparticles on the sensing properties of the single ZnO -T or its arm. In a previous work [27], the ZnO -T networks alloyed with Fe_2O_3 micro- and nanoparticles demonstrated poor UV and gas sensing properties. Thus, the potential to improve the sensing properties based on single structures is investigated in this work.

Here, we present UV and gas sensing investigations of single Fe-doped ZnO -T, multiple Fe-doped ZnO -T and single Fe_2O_3 -alloyed ZnO -T. The influence of relative humidity on the gas sensing properties was investigated, which revealed an improved stability to high RH values. A responsible gas sensing mechanism was proposed and discussed in detail. The devices based on single Fe-doped ZnO -T and Fe_2O_3 -alloyed ZnO -T with improved sensing properties were compared to pristine single ZnO -T as an essential step in nanotechnology of sensing devices based on single 3-D micro- and nanostructures.

2. Experimental part

2.1. Growth, characterization and sensing measurements

The synthesis process and morphological, structural, optical and chemical characterization of the ZnO -T networks alloyed with Fe_2O_3 were reported in detail in previous work [27,28]. The ZnO -T networks were synthesized by flame transport synthesis (FTS) [28], while alloying was achieved by homogenous mixing of the ZnO -T with Fe microparticles (diameter $<10\text{ nm}$, GoodFellow UK 99%) and further annealing at 1150°C for 5 h [28]. This work is mainly focused on the investigations of UV and ethanol vapour sensing properties of the devices based on single 3D ZnO -T. Device fabrication was performed in a FIB/SEM system using the procedure described by Lupan et al. [2]. The UV and gas sensing investigations were performed as reported previously [20,29]. The intensity of the UV light source ($\lambda = 365\text{ nm}$) was set to $15\text{--}20\text{ mW cm}^{-2}$ and the UV sensing investigations were performed in air under normal ambient conditions ($\approx 30\%$ RH) in the dark. The gas sensing measurements were performed at room temperature at $\approx 30\%$ and $\approx 70\%$ RH, which was set using a bubbling system and was measured using a standard hygrometer [29]. The target gas was mixed with ambient air using pre-calibrated mass flow controllers (MFC, Bronkhorst UK) in order to obtain the necessary concentration. The UV and gas response were measured and processed as reported previously [5]. The responsivity (R) and the internal photoconductive gain (G) are important parameters to indicate the performances of the photodetectors and were calculated using the following equation [30]:

$$R = \frac{I_{ph}}{P_{opt}} = \frac{q}{hc} G \quad (1)$$

where I_{ph} is photocurrent ($I_{UV} - I_{dark}$), P_{opt} is the incident optical power of the UV source, q is the quantum efficiency, h is Planck's constant, c is the speed of light, λ is the wavelength of UV light (365 nm). The current through the fabricated devices was continuously monitored and recorded using a computer-controlled Keithley 2400 source meter through a LabView software (National Instruments). In the case of UV sensing measurements, different bias voltages were applied in order to investigate the influence on the response and rapidly, while in the case of gas sensing measurements the applied bias voltage for all measurements was set to 1 V in order to minimize the self-heating effect.

2.2. Computational details

Spin polarized Density Functional Theory (DFT) calculations with the plane-wave pseudo-potential method [31,32] were performed, as implemented in the Vienna Ab-initio Simulation

Package (VASP) [32]. We have used our earlier DFT optimized structures of different molecules interacting with the Fe₂O₃-doped ZnO(0001) surface, where the geometries were optimized using the tetrahedron method with the Blöchl correction [33], whereas the implementation of the DFT-D2 approach described by Grimme [34] was used to account for long-range dispersion forces. Other computational details are the same as described in detail in our previous work.

A Bader charge analysis was carried out, using the code developed by Henkelman and co-workers [35,36], to calculate the charge transfer between the surfaces and different molecules. Bader charges and electronic charge densities were calculated using a relatively dense $9 \times 9 \times 1$ Monkhorst-Pack [37] k-point mesh with a tetrahedron smearing parameter of 0.2 eV and a Self-Consistent-Field (SCF) convergence criterion of 1×10^{-6} eV per unit cell.

3. Results and discussions

3.1. Morphological and chemical properties of Fe-doped and Fe₂O₃-alloyed ZnO-T networks

The SEM images of the synthesized ZnO-T networks alloyed with Fe₂O₃ NPs and MPs are presented in Fig. S1 in Supplementary material. In this work three types of devices were fabricated based on single structures from ZnO-T networks alloyed with Fe₂O₃ at relatively low (see Fig. S2(a,b)) and higher concentrations (see Fig. S2(c-f)), by gradual dispersion from higher to lower concentrations. It can be observed that the Fe₂O₃ NPs and MPs are randomly distributed and do not detach from the ZnO-T after the dispersion and a transfer process to the SiO₂/Si substrate (see Fig. S2(f)) for the further integration into devices using a FIB/SEM system [2,20]. In a previous work it was demonstrated that during the synthesis process, beside the formation of Fe₂O₃/ZnO heterostructures by Fe₂O₃ NPs and MPs on the surface of ZnO-T, the ZnO-T are also doped with Fe in the same synthesis process of the samples [27]. The composition of NPs on the surface of ZnO-T was also analysed with EDX-line scan and elemental mapping. The EDX spectrum of a single microparticle transferred together with ZnO-T onto a Si substrate showed a [O]:[Fe] ratio of 1.5, which fits very well with Fe₂O₃ (see Fig. S3(a)). The content of Fe in ZnO-T was determined at 0.14 at.% (see Fig. S3(b)). Results of EDX-line scan and elemental mapping are presented in Fig. S4. In this work we have mainly investigated the effect of Fe-doping and the influence of Fe₂O₃ nanoparticles and MPs on the sensing performances of the single ZnO-T. The fabricated devices are denoted by device 1, 2 and 3.

3.2. Single Fe-doped ZnO-T

Device 1 is fabricated based on a single Fe-doped ZnO-T (see Fig. 1(a,b)). One leg of the ZnO-T is contacted by Pt to one Au pad. Two other legs are contacted to a second Au pad, and the fourth leg is pointing in the air (see Fig. 1(b)). The diameter of the tetrapod leg at its end is ≈ 800 nm while at the base of the tetrapod it is ≈ 1.2 μ m. The length of the legs is ≈ 4 μ m. The current-voltage characteristic of Device 1 is presented in Fig. S5(a), showing an almost symmetric nonlinear characteristic caused by the formation of double Schottky contacts at the interface between Pt and the ZnO-T legs due to the higher work function of Pt compared to ZnO [38]. The device was exposed to UV light under different applied bias voltages. The calculated UV response is presented in Fig. 1(c), showing an improved UV response compared to pristine single ZnO-T reported earlier by Lupan et al. [2]. An increase in UV response by doping with Fe was also observed for ZnO nanostructured films [5] and was attributed to induced defects which enhance the oxygen adsorption onto the surface of ZnO, and respectively improve the UV response [5,39].

Another reason could be the improved surface-to-volume ratio of the Fe-doped ZnO-T tetrapod due to the layered morphology of the arms (Fig. 1(a,b)), which can lead to a higher coverage by oxygen species. By increasing the applied bias voltage, a decrease in the UV response was observed (see Fig. 1(c)), which was also observed for ZnO-T networks [40] and single Ag-doped ZnO NW [41]. At 1 V applied bias voltage, Device 1 demonstrated an UV response of 18, while at 25 V applied bias voltage the UV response decreased to ≈ 2 .

The dynamic UV response at different applied bias voltages with two applied UV pulses for the duration of 10 s is presented in Fig. 1(d) and in Fig. S6 (in logarithmic plot). The dynamic measurements at 1 V and 5 V applied bias voltage demonstrated that the photocurrent of Device 1 not fully recovers to its initial electrical baseline after switching off the UV light, demonstrating the existence of persistent photoconductivity (PPC). In the case of single nano- and microstructures of metal oxides the PPC is directly related to the electron-hole separation near the surface, and after illumination the charge separation makes the electron-hole recombination difficult and originates PPC [42]. However, at higher applied bias voltages, the PPC effect is considerably reverted probably due to a self-heating effect [42]. For demonstration of the device rapidity, short pulses with a duration of ≈ 0.5 s were also applied, shown in Fig. 1(e), which shows the rapid increase and decrease of photocurrent for a rapid switch of UV light source. Thus, Device 1 can work relatively fast, compared to previously reported results [2]. To better investigate the rapidity of the device the time constants of the response and recovery times were calculated and are generalized in Fig. 1f and Table S1. In conclusion, the slow component of the response time (τ_2), corresponding to photo-desorption of oxygen molecules [5,41], increases with an increase of the applied bias voltage, while other time components are decreasing (see Table S1). This tendency is similar to the results reported for single ZnO:Ag NW [41], and can be attributed to temperature-dependent photo-desorption/adsorption processes as a result of self-heating effects of single structures [25]. However, in the case of ZnO:Ag NW the dependence of time constants on the applied voltage is stronger due to the smaller diameter of the structure ≈ 300 nm [41] and a more pronounced self-heating effect [25,41]. In the case of the tetrapod from Device 1 (see Fig. 1(a,b)) due to the leg diameter of ≈ 800 nm the self-heating effect is lower but on the other hand the fabricated devices can support relatively high applied bias voltage and current values (see Fig. S5(a)), which add flexibility to other electronic applications.

The calculated R and G versus applied bias voltage for Device 1 are presented in Figs. 2 and S7(a), assuming $\beta = 1$ for simplicity. Low values of $G < 1$ in the whole range of applied bias voltages indicate the absence of an internal photoconductive gain. Because G is dependent on photocarrier lifetime and carrier transit time, the low G value can be attributed to the relatively high dimensions of the tetrapod, i.e. big diameters of the arms and distance between contacts [43].

In conclusion, the device based on Fe-doped ZnO-T demonstrated improved UV sensing performance compared to pristine ZnO-T [2] with a high stability and relatively fast UV response with good repeatability. At lower applied bias voltage (1 V) an incomplete recovery was obtained, but by increasing the applied bias voltage the recovery time decreased considerably, showing a complete recovery to the initial baseline, which is quite important for real applications. In another section, we will present a comparison of all three devices.

3.3. Interconnected Fe-doped ZnO-Ts

Device 2 is based on two Fe-doped ZnO-Ts with different dimensions and without alloyed Fe₂O₃ nanoparticles (see Fig. 3 and Fig. S8). One Pt contact was formed at the end of the biggest tetra-

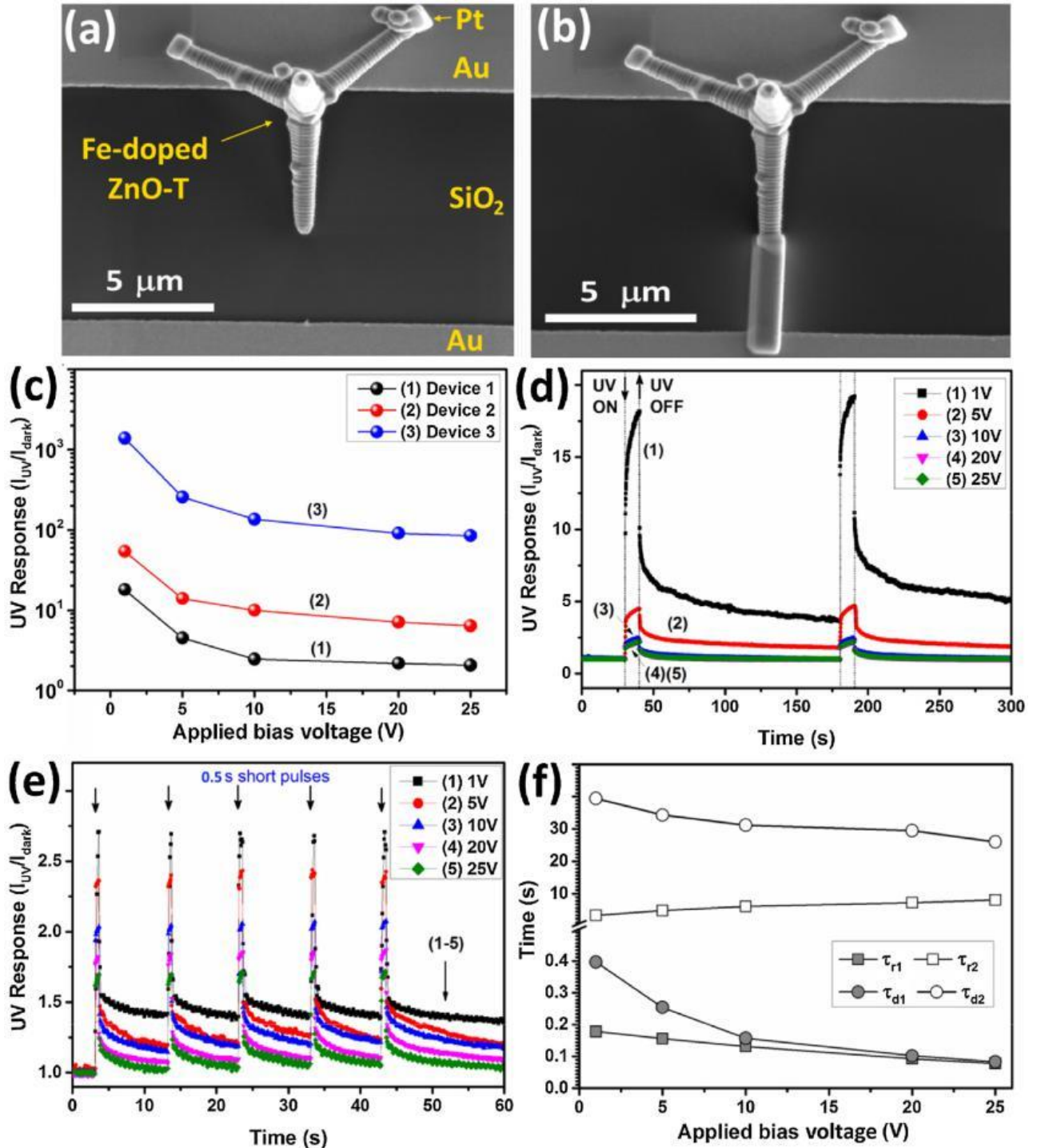


Fig. 1. (a,b) SEM image of Device 1 before and after deposition of Pt contacts in FIB/SEM system. (c) UV response versus applied bias voltage of the fabricated devices. (b) Dynamic UV response at different applied bias voltages of Device 1. (e) Dynamic UV response at different applied bias voltages to short UV pulses of ≈0.5 s of Device 1. (f) Calculated time constants for response and recovery curves by bi-exponential fitting for different applied bias voltages of Device 1 (τ_{r1} , τ_{r2} for response curve and τ_{d1} , τ_{d2} for recovery curve).

pod (see inset from Fig. 3(a)) and another Pt contact was formed at the arm of the other tetrapod (see Fig. S8(c)). The diameters of the tetrapod legs slightly vary along the length for both tetrapods (see Fig. 3(a) and Fig. S8(a,b)). The diameter of the legs of the bigger tetrapod is ≈3.5 μm, while of the smaller one is ≈2.7 μm, and the length of the tetrapod legs are ≈24.8 μm and 10.5 μm for the bigger and smaller one, respectively. The diameters are higher than for Device 1. The tetrapods are well interconnected at the end of their

arms (see Fig. 3(b)). The current voltage characteristic is presented in Fig. S5(b), showing the double Schottky characteristic.

Even if the diameters of the tetrapod legs of Device 2 are bigger, this device demonstrated a higher UV response compared to Device 1 (see Fig. 1(c)). For example at 1 V applied bias voltage the UV response is 54, compared with that of 18 by Device 1. Also, no PPC was observed at lower applied bias voltages, as was the case in Device 1. The main reason will be discussed in the section about the

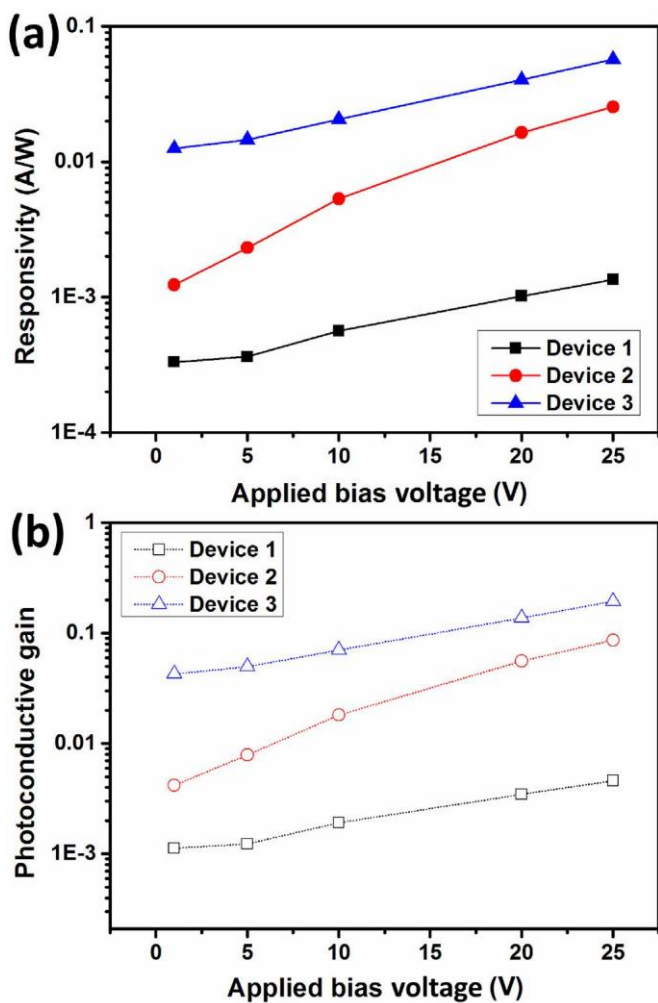


Fig. 2. Dependence of (a) responsivity (R , A/W) and (b) photoconductive gain (G) on applied bias voltage for Devices 1, 2, and 3.

sensing mechanism and is based on the junction that have formed between the tetrapods, which can essentially enhance the sensing properties of the device [44].

Fig. 3(c,d) shows the dynamic UV response and the calculated time constants, respectively, of Device 2 under different applied bias voltages. Device 2 showed a much shorter recovery time compared to Device 1, while the response time constants are almost similar, indicating an improved rapidity of the device through the formation of junctions between the tetrapods. Thus, it can be concluded that additional junctions can improve not only the UV response, but also the rapidity of the sensors. More evidence for this scenario is shown in the case of multiple junctions between ZnO tetrapods. For example, Gedamu et al. reported a response for nano-tetrapod networks of about 4.5×10^3 under UV light illumination with $\sim 45 \text{ mW cm}^{-2}$ at an applied bias voltage of 2.4 V with a rise and decay time of $\sim 67 \text{ ms}$ and $\sim 30 \text{ ms}$ [40]. Thep-nurat et al. reported a response for inter-linked ZnO tetrapod networks a response of about $7.4 \cdot 10^3$ under UV light illumination with 2.8 mW cm^{-2} at 5 V at an applied bias voltage of 5 V with a rise and decay time of 3.52 s and 0.67 s [45]. The mechanism responsible for these findings will be discussed in the section on gas sensing. The calculated R and G parameters for Device 2 are presented in Figs. 2 and S7(b), and are higher than those of Device 1. In conclusion, for the first time a device based only on two interconnected T was fabricated. Even for much higher diameters of the tetrapod legs, of the order of several micrometers, the UV response can be enhanced due

to the formation of a junction between the two tetrapods, which is a highly efficient way to improve the sensing performance of the device [44].

3.4. Single Fe-doped ZnO-T alloyed with Fe_2O_3

Figs. 4 a and 5 show the SEM images of Device 3 and other devices, respectively, based on Fe-doped ZnO-T alloyed with Fe_2O_3 micro- and nanoparticles. Other devices demonstrated the same tendency in UV and gas properties as Device 3, and in order to avoid agglomeration in this paper of almost similar data, only the UV and gas sensing properties of Device 3 will be presented. It can be observed that spherical micro- and nanoparticles are attached on the surface of the ZnO-T (see Figs. S9 and 5). In a previous work it was shown that these nanoparticles are composed of Fe_2O_3 [27]. The overall SEM image of Device 3 is presented in Fig. S9(a), with magnified SEM images of the ZnO-T from Device 3 showing the attached micro- and nanoparticles (see Fig. S9(b-c)). The Pt contacts are presented in Fig. S9(e,f), which show that whereas one Pt contact is formed at the end of the longest tetrapod leg, a second contact was formed at another leg, to include the base of the tetra-pod into the sensing process. It can be observed from Fig. S9(d,e) that many Fe_2O_3 micro- and nanoparticles are attached at the base of ZnO-T, which can positively influence the sensing properties of the devices. The current-voltage characteristic of Device 3 in the dark is presented in Fig. S5(c), which shows the same double Schottky characteristics as for Devices 1 and 2. The lengths of the tetrapod legs are $\approx 33 \text{ m}$ and 19 m . The diameter of the tetrapod leg at the end is $\approx 1.2 \text{ m}$ while at the base of the tetrapod is $\approx 2.3 \text{ m}$. These geometrical parameters are higher than for Device 1 and lower than for Device 2.

Fig. 1(c) shows the UV response of Device 3 versus the applied bias voltage, which shows a similar tendency compared to Devices 1 and 2, i.e. a decrease in UV response with an increase of applied bias voltage. However the UV response for Device 3 is about 80 times higher than for Device 1 and about 25 times higher than for Device 2, demonstrating exceptional UV sensing improvements by alloying with Fe_2O_3 micro- and nanoparticles. For example at an applied bias voltage of 1 V, the UV response increased from 18 for Device 1 to ≈ 1400 for Device 3. Taking into account that the diameter of the tetrapod legs of Device 3 is larger than in Device 1, the most probable responsible mechanism for the improved UV sensing properties can be attributed to the influence of the Fe_2O_3 micro- and nanoparticles, which will be discussed in the relevant section.

The dynamic UV response with applied UV pulses of 10 s and a shorter 0.5 s at different applied bias voltages is presented in Fig. 4b and in Fig. S10 (in the logarithmic plot). Compared to Device 1 (see Fig. 1d) the current recovers more rapidly to its initial electrical baseline. The calculated time constants of the response and recovery curves of the dynamic UV response are presented in Fig. 4c and Table S1. An example of bi-exponential fitting of the photoresponse rise and decay curves is presented in Fig. S11. The same tendency on the applied bias voltage was observed as in the case of Devices 1 and 2 (see Fig. 1f). The calculated R and G for Device 3 are about one order of magnitude higher than for Device 1 (see Fig. 2), although the G value is still lower than 1 indicating on the same absence of internal photoconductive gain for the same reasons as in Devices 1 and 2.

In conclusion, by alloying Fe-doped ZnO-T with Fe_2O_3 micro- and nanoparticles, an increase in UV sensing properties, including UV response and rapidity, can be obtained even for tetrapods with a larger diameter of their legs. Thus, alloying the single structures with other semiconducting oxides is an important strategy to improve UV sensing properties of the devices based on single structures with micrometer size. Table 1 shows the other results for UV photodetectors reported in the literature based on single micro-

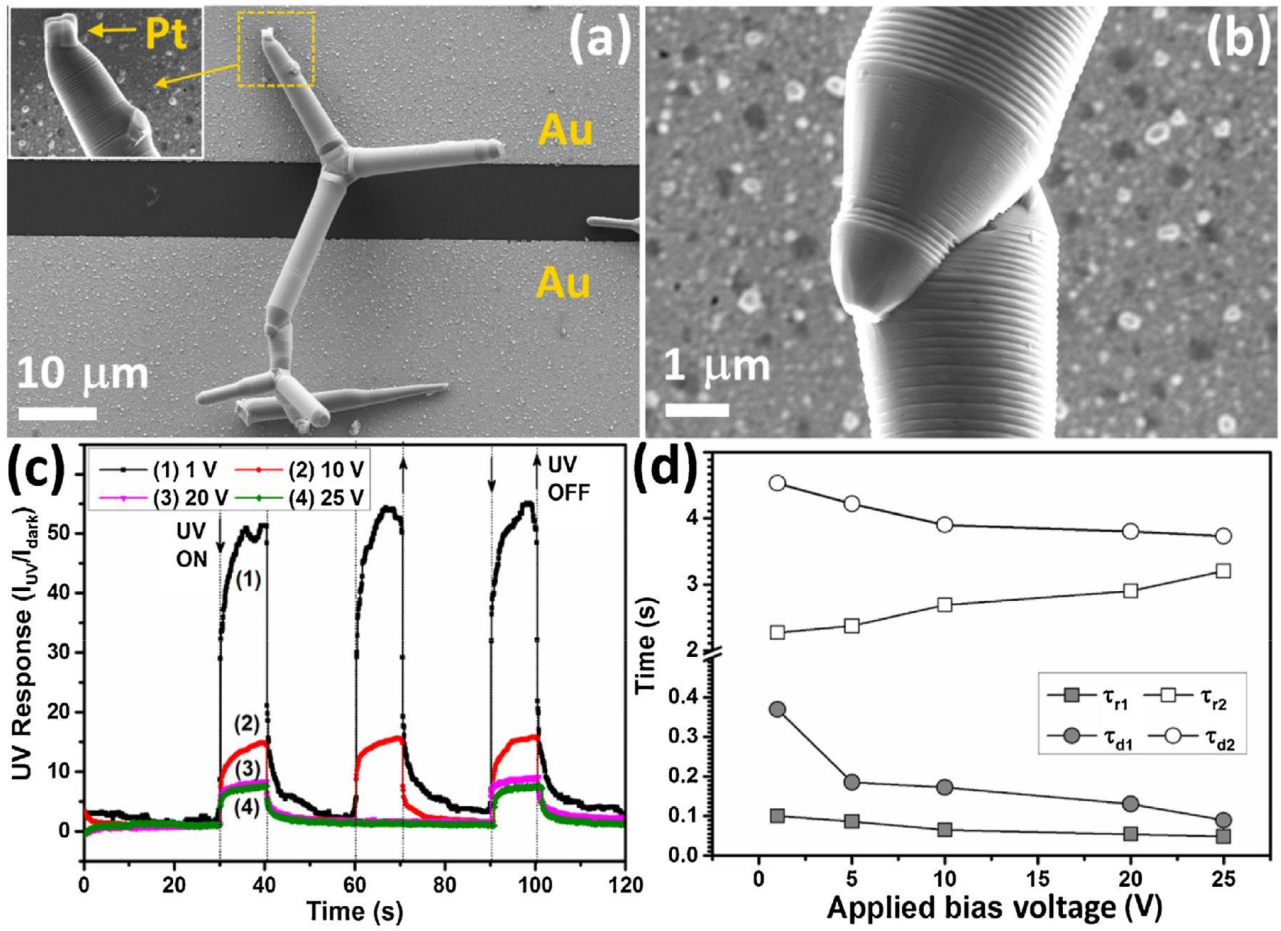


Fig. 3. SEM images of Device 2: (a) overall view of the integrated two tetrapods, bigger one and smaller one, which are interconnected. In inset a magnified view of one Pt contact is presented; (b) Interconnection of the tetrapods. (c) Dynamic UV response at different applied bias voltages. (d) Calculated time constants for response and recovery curves by bi-exponential fitting for different applied bias voltages (τ_{r1} , τ_{r2} for response curve and τ_{d1} , τ_{d2} for recovery curve).

Table 1
Parameters of UV photodetectors based on single semiconducting oxide nanostructures.

Sensing material and properties	(nm)	Power of UV illumination (mW/cm ²)	UV on-off ratio	Response/rise time (s)	Recovery/decay time (s)	Year of pub.
Single ZnO nanobelt coated with polystyrene sulfate [7]	280	–	$7.5 \cdot 10^4$	–	–	2007
ZnO functionalized SnO ₂ NW [26]	365	–	1.5	>100 s	>100 s	2008
Single ZnO-T [2]	361	0.7	1.035	45	23	2009
Single ZnO MW [59]	365	0.1	≈ 1.012	>100 s	>100 s	2011
Single ZnO NW phototransistor [60]	360	–	≈ 100	–	–	2011
ZnO NW with Schottky barrier [61]	365	7.6	$4 \cdot 10^5$	–	$d1 \approx 0.046$	2011
ZnO MW [62]	325	24	$9 \cdot 10^5$	20	$d1 \approx 0.85$	2013
Au-decorated ZnO NW [63]	350	20	$2.89 \cdot 10^6$	$r1 \approx 0.4$	$d1 \approx 1.5$	2015
Single Ga ₂ O ₃ /GaN:O _x @SnO ₂ NB [64]	–	5	≈ 10	0.1	0.1	2015
Single Ag-doped ZnO NW [41]	365	15–20	52	1.09	5	2016
Fe-doped ZnO-T (device 1), 1 V	365	15–20	18	$r1 \approx 0.178$ $r2 \approx 3.3$	$d1 \approx 0.396$ $d2 \approx 39.4$	This work
Two interconnected Fe-doped ZnO-T (device 2), 1 V	365	15–20	54	$r1 \approx 0.1$ $r2 \approx 2.27$	$d1 \approx 0.369$ $d2 \approx 4.53$	This work
Fe-doped ZnO-T alloyed with Fe ₂ O ₃ micro- and nanoparticles (device 3), 1 V	365	15–20	$\approx 1.4 \cdot 10^3$	$r1 \approx 0.31$ $r2 \approx 1.74$	$d1 \approx 1.2$ $d2 \approx 8.7$	This work

and nanostructures of semiconducting oxides in order to compare with our results. It can be observed that the device based on Fe-doped ZnO-T alloyed with Fe₂O₃ micro- and nanoparticles shows high UV sensing performances.

3.5. Gas sensing properties

Taking into account that previous studies have revealed improved ethanol vapour (EtOH) detection properties of the Fe-doped ZnO nanostructured films [5], in this study the gas sensing properties at room temperature of the fabricated devices were also

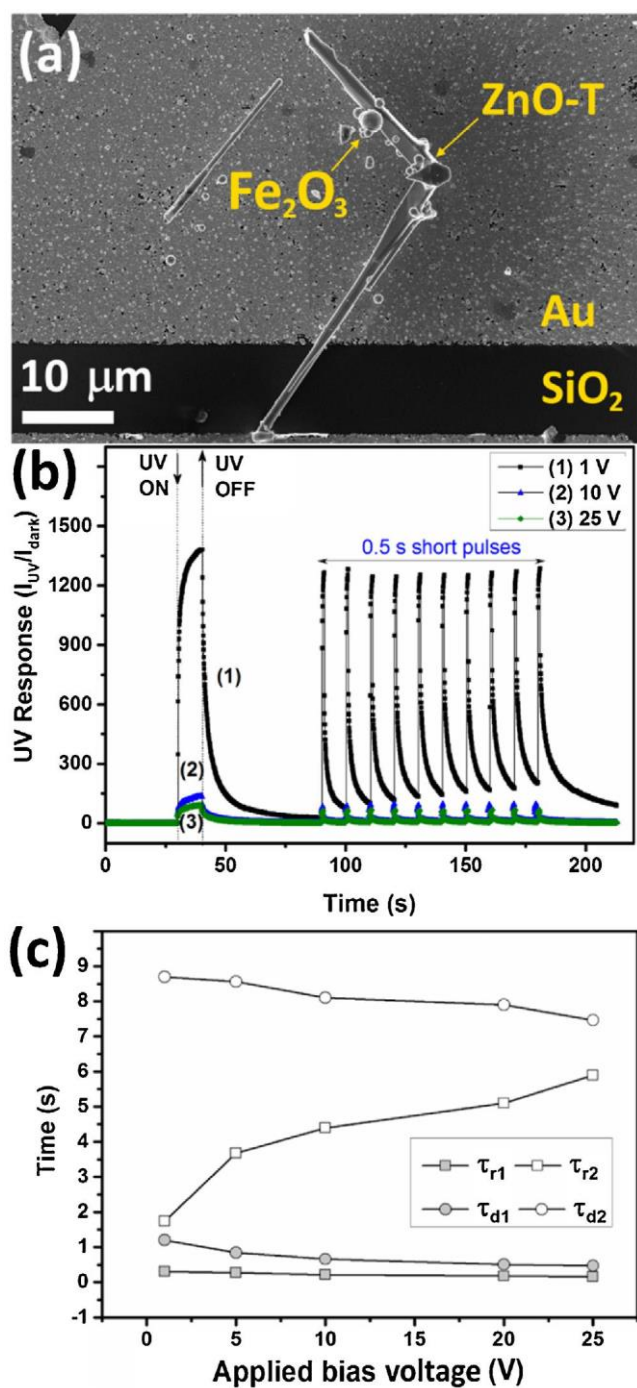


Fig. 4. (a) SEM images of Device 3 based on Fe-doped ZnO-T alloyed with Fe₂O₃ micro- and nanoparticles contacted to Au pads. (b) Dynamic UV response at different applied bias voltages. (c) Calculated time constants for response and recovery curves by bi-exponential fitting for different applied bias voltages (τ_{r1} , τ_{r2} for response curve and τ_{d1} , τ_{d2} for recovery curve).

investigated. As indicated in the experimental part, in the case of gas sensing measurements the applied bias voltage for all measurements was 1 V in order to minimize the self-heating effect. Thus, the current in air is of order of nA (0.1–5 nA, see Fig. S5). Although the self-heating effect becomes a critical concern in nano-scaled devices, in our case the diameter of tetrapod legs in the range of 800 nm–3.5 μm, which is out of the nanoscale dimensions and the self-heating effect is therefore negligible [25].

Fig. 6(a) shows the gas response at room temperature of Devices 1, 2, and 3 to three reducing gases (EtOH, H₂ and CH₄) with a con-

centration of 100 ppm at 30% and 70% RH. No response to CO gas was observed and this was therefore not included in the graphs. A decrease in sensing performances at higher value of RH was observed (see Table S2), which is typical for semiconducting oxide nanostructures due to the adsorption of water [1,3,29]. All devices demonstrated an excellent selectivity to EtOH. The EtOH response

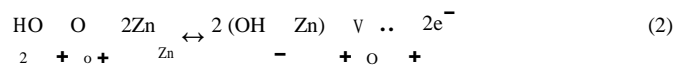
(S_{EtOH}) for Devices 1, 2, and 3 are 9, 16.5, and 51, respectively (to 100 ppm). Thus, as in the case of UV sensing properties, Device 3 demonstrated the highest EtOH sensing properties, i.e. gas response and selectivity. For example the ratio of EtOH and H₂ responses

(S_{EtOH}/S_{H_2}) for Devices 1, 2, and 3 are ≈ 7 , ≈ 7.8 , and ≈ 20 , showing a distinct improvement in selectivity as a result of alloying Fe-doped ZnO-T with Fe₂O₃ micro- and nanoparticles. For the doped structures the same value for the selectivity is observed, revealing that additional junctions between tetrapods have no impact on the selectivity, but only on the gas sensing potential of the device (see Fig. 6(a)). In general, such excellent gas sensing performances can be attributed to a layered structure of the arms of the tetra-pod, which increase the surface-to-volume ratio of the structure and lead to higher gas responses.

Fig. 6(b) shows the EtOH response of Device 3 versus the concentration of EtOH (p_{EtOH}), showing a typical power law dependence $S_{EtOH} \propto p_{EtOH}^{\gamma}$, where $\gamma = 0.587$ is the slope of $\log S_{EtOH}$ vs. $\log p_{EtOH}$ [29]. The lowest detection limit (LDL) for EtOH detection of Device 3 was approximated by linear fitting of $\log S_{EtOH}$ vs. $\log p_{EtOH}$ dependence with response criteria $I_{gas}/I_{air} > 1.2$, and was found to be ≈ 0.2 ppm (see Fig. 6b).

The dynamic EtOH response to 50 ppm and 500 ppm of Device 3 are presented in Fig. 6(e) and in the inset of Fig. 6(f), respectively. The calculated response and recovery times for different concentrations of EtOH at 30% RH are presented in Fig. 6(f) and Table S3, showing a decrease in response and recovery time with an increase in EtOH concentration. The dynamic response of Devices 1 and 2 are presented in Fig. 6(c,d). These devices demonstrated much slower response and recovery times (see Table S2), revealing that alloying with Fe₂O₃ can significantly improve the rapidity of sensors based on single structures.

Next will be discussed the influence of higher values of RH on the sensing performances of the devices. When increasing the RH value from 30% to 70%, the EtOH response of Devices 1, 2, and 3 decreases by $\approx 47\%$, $\approx 45\%$, and $\approx 17\%$ (see Table S2). The dynamic EtOH response of the devices at 70% RH is presented in Fig. S12. It can be observed, that besides the decrease in gas response (see Fig. 6(a)), a decrease in rapidity of the sensors occurs with an increase in the RH value from 30% to 70%. All calculated parameters (gas response with recovery and response time) at 30% and 70% RH are presented in Tables S2 and S3. It can be concluded that alloying Fe-doped ZnO-T with Fe₂O₃ has reduced the gas sensing dependence on the humidity, which can be related to the influence of the Fe₂O₃ micro- and nanoparticles and not the Fe-doping of ZnO-T. For example, the recovery time of Devices 1 and 2 increases about 2 times for 70% RH, while for Device 3 an increase in recovery time from 12.3 s to 15.7 s was observed. A better indicative factor is the decrease in gas response by only $\approx 17\%$ for 70% RH compared with $\approx 45\%$ for Devices 1 and 2. Such decrease is attributed to water molecules (H₂O) adsorbing onto the surface of the tetrapods [1,3,29,46]. The reaction of H₂O with lattice Zn_{Zn} can be described as follow [46]:



where OO is the lattice oxygen and VO is the vacancy created at the oxygen site. This reaction is reversible with a donor effect, leading to a decrease of device resistance [46]. Together with this effect, exposure to humidity adds competition for adsorbed oxygen molecules between the EtOH molecules and water molecules, lead-

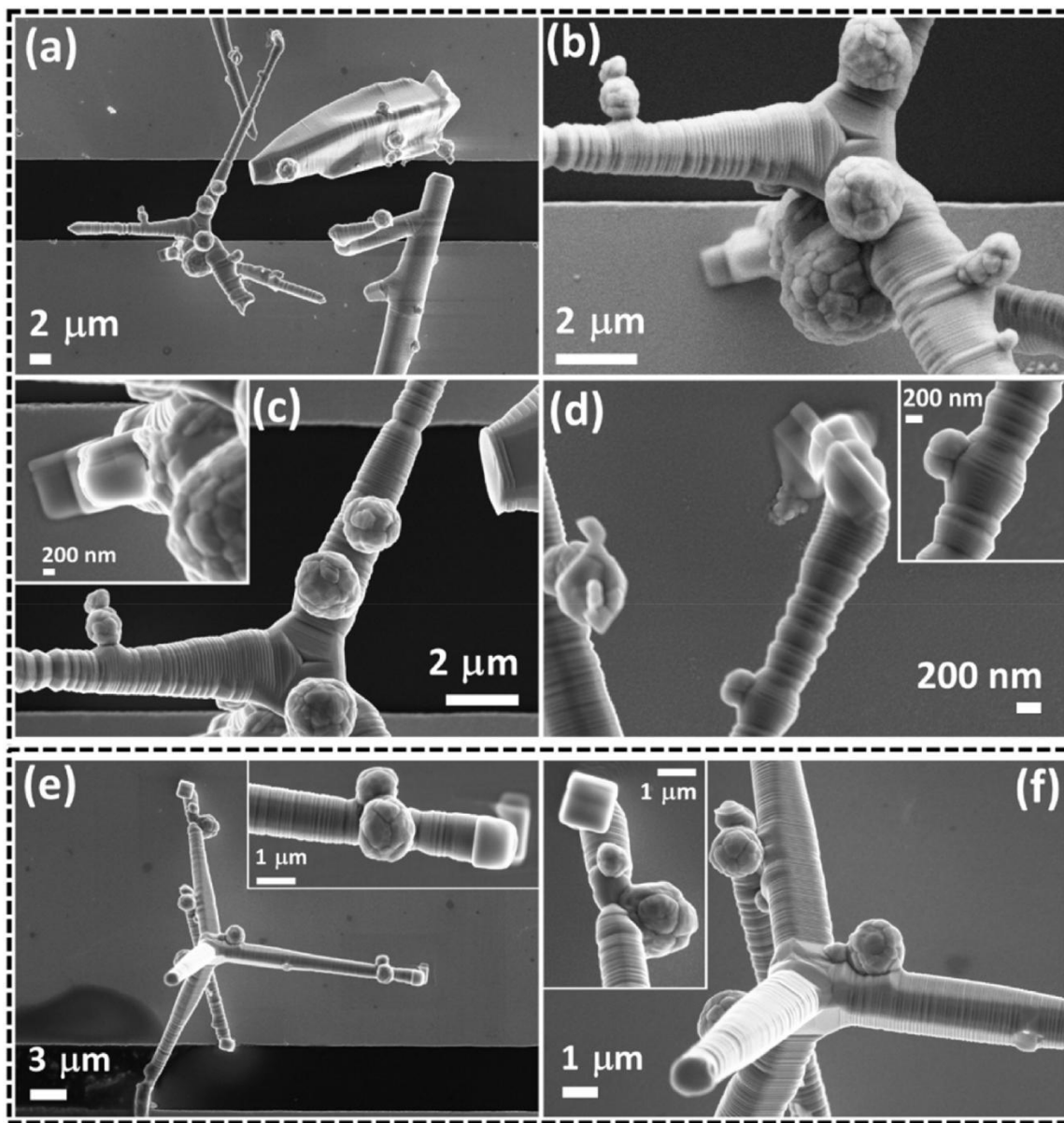


Fig. 5. SEM images of other devices based on Fe-doped ZnO-T and other structures alloyed with Fe₂O₃ micro- and nanoparticles: (a) overall view at low magnification; (b,c) surface of the ZnO-T to demonstrate the attached Fe₂O₃ micro- and nanoparticles. In inset a Pt contact is presented. (d) Other Pt contact at one end of T arm. In inset a Fe₂O₃ micro- and nanoparticle attached to a T arm is presented. (e,f) Another device at lower and higher magnifications is shown. In inset Pt contacts are presented.

ing to a decrease in sensor response [3,29]. The reduced humidity dependence of the gas sensing characteristics was also observed for NiO-doped SnO₂ nanostructures [3], where NiO played an important role as a strong humidity adsorber. Because Fe₂O₃ nanostructures are known to be efficient humidity sensors [47], we believe that in our case the role of adsorber is performed by the Fe₂O₃ nanoparticles, which prevent the reaction of water molecules with Fe-doped

ZnO-T. For example the RH response ($I_{30\%RH}/I_{70\%RH}$) of Devices 1 and 2 is ≈ 2.1 , while for Device 3 it is ≈ 1.3 (not shown). Kovalenko et al.

[18] also observed that ethanol vapour response of SnO₂/Fe₂O₃ nanocomposites is independent of RH.

Table 2 shows the ethanol vapour sensor parameters of other single structures of semiconducting oxides. It can be observed that the Fe-doped ZnO-T alloyed with Fe₂O₃ micro- and nanoparticles shows exceptionally improved ethanol vapour sensing properties among the devices fabricated using individual micro- and nanostructures. The response of Device 3 is comparable with recently reported results for Fe₂O₃ NPs-SnO₂ NWs (gas response of R_{air}/R_{gas}

≈ 57.56 –200 ppm of ethanol), which has a much higher optimal operating temperature of 300 °C and lower rapidity (response time ≈ 65 s and recovery time ≈ 220 s) [16], and with ZnO/Fe₂O₃ hierarchical nanostructures (gas response of $R_{air}/R_{gas} \approx 53.6$ to 100 ppm of ethanol) with an optimal operating temperature of 300 °C and higher rapidity (response time ≈ 6 s and recovery time ≈ 7 s) [12].

3.6. Sensing mechanism

The ethanol vapour sensing mechanism based on ionosorption/desorption of oxygen species was described in our previous work [1,5,41]. The UV sensing mechanism of the pristine and alloyed ZnO-T was also reported [2,5,27], which is based mainly on the modulation of the surface space charge region (SCR) under adsorption/desorption of gaseous species. Thus in this work we will focus mainly on the effect of the junction formed between tetrapods and the Fe₂O₃ alloying effect.

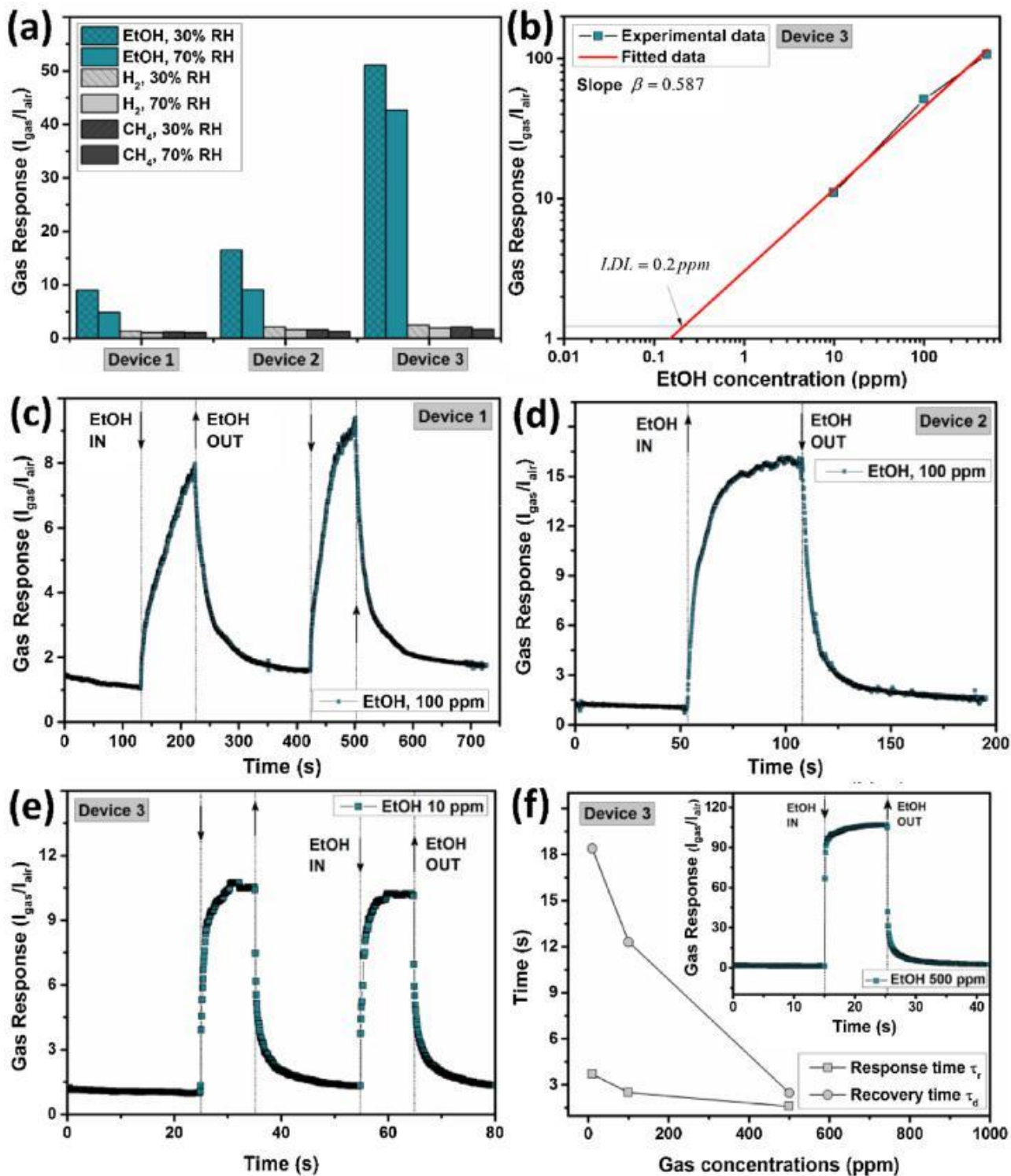


Fig. 6. (a) Room temperature (RT) gas response of the devices for different reducing gases at 30% and 70% RH. (b) Gas response versus EtOH concentration. Dynamic EtOH response at RT and at 30% RH of: (c) Device 1–100 ppm; (d) Device 2–100 ppm; and (e) device 3–100 ppm. (f) Response and recovery time versus gas concentration. In inset a dynamic EtOH response at RT to 500 ppm at 30% RH is presented.

Improved UV and gas sensing properties of Device 2 compared with Device 1, i.e. sensing properties of interconnected tetrapods compared to a single tetrapod (see Fig. 7(a)), can be explained based on an additional potential barrier that has formed (qV_{S1} , see Fig. 7(b)), which dominates the sensing properties of the device [48]. Under exposure to ambient air oxygen molecules adsorb onto the surface of the tetrapods ($O_2(g) + e^- \rightarrow O_2^-(ads)$) [2,41,49]), form-

ing the surface space charge region (see Fig. 7(a)) [2,41,49]. In both cases, i.e. at illumination with UV light or exposure to ethanol molecules, the height of the potential barrier between tetrapods is decrease (qV_{S2} , see Fig. 7(b)). Thus, the additional potential barrier formed leads to a more efficient modulation in device resistance [44,50], while in the case of a single tetrapod the change in resistance occurs only by modulation of the SCR width under influence

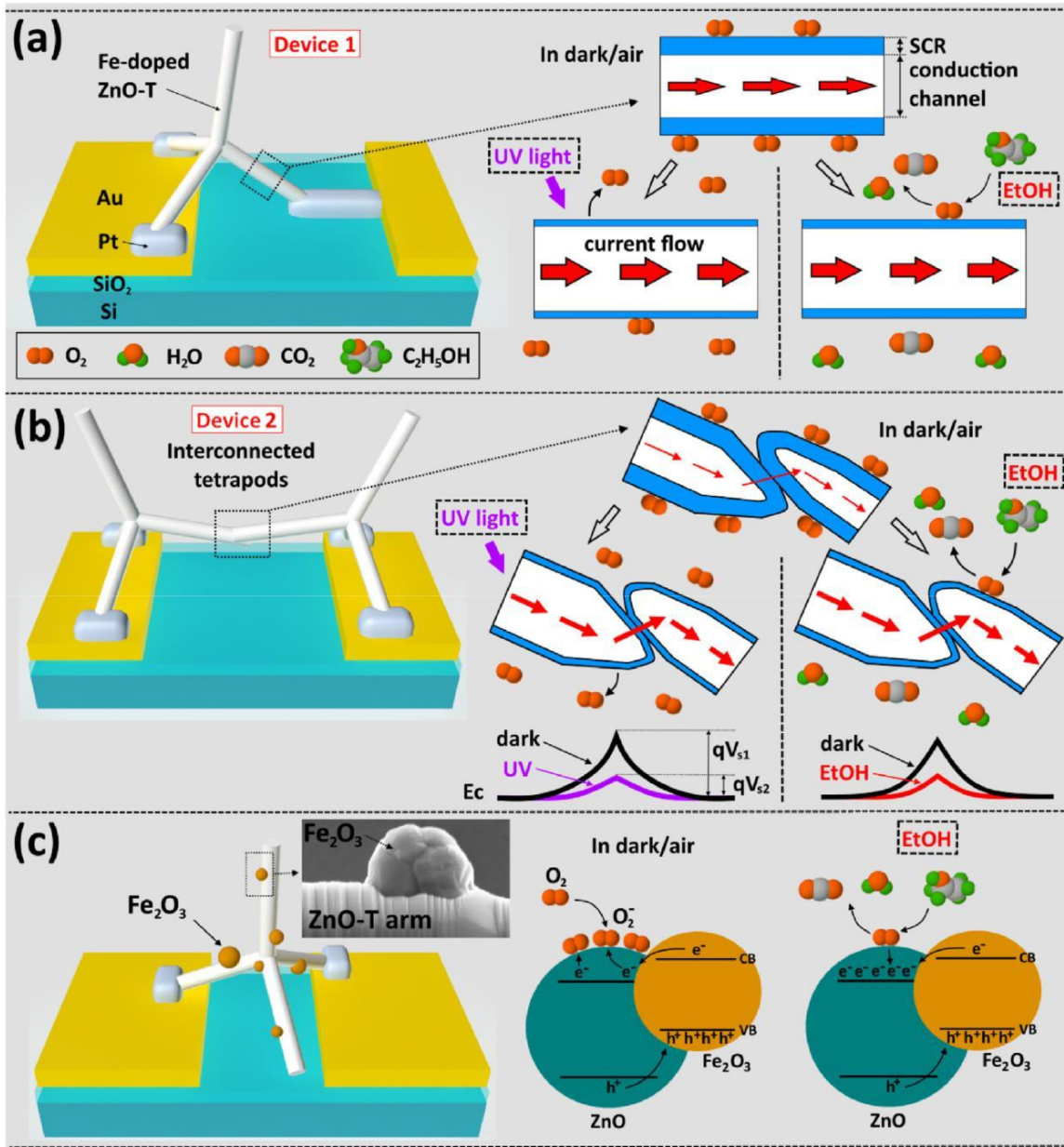


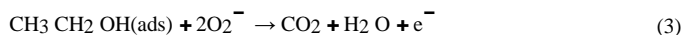
Fig. 7. UV and ethanol vapour mechanism of Devices: (a) 1; (b) 2; and (c) 3. (a) On the left side a schematic illustration of Device 1 based on Fe-doped ZnO-T is presented. At the exposure in air the oxygen molecules are adsorbed onto the surface of the tetrapod and create a SCR region. At the exposure to UV light the photodesorption process occurs and decreases the width of the SCR region, leading to an increase of current through the T arm. At the exposure to ethanol molecules, the decrease in width of SCR region occurs due to released electrons after the oxidation reaction of molecules to H₂O and CO₂ molecules. (b) On the left side a schematic illustration of Device 2 based on two interconnected T is presented. The main mechanism is based on modulation of the potential barrier (qV_{S1} decrease to qV_{S2}) between arms in the case of UV illumination and exposure to ethanol molecules. (c) On the left side a schematic illustration of Device 3 based on single Fe-doped ZnO-T alloyed with Fe₂O₃ nanoparticles is presented. In inset a SEM image of the Fe₂O₃/ZnO-T arm heterojunction is presented. At the surface of ZnO more oxygen molecules adsorb leading to higher modulation in resistance (charge transfer) after exposure to ethanol molecules.

of UV light or gases [2], which is less significant for tetrapod arms with relatively high diameter (Device 1, see Fig. 7(a)).

In the case of UV illumination of Device 2 the decrease in potential barrier height is due to photogenerated electron-hole pairs ($h\nu \rightarrow e^- + h^+$) and subsequent photodesorption of oxygen molecules ($O_2^-(ads) + h^+ \rightarrow O_2(g)$, see Fig. 7(a,b)) [2,5,20,41,49]. The increase in UV sensing properties, especially the rapidity, of the single structure through the formation of an additional potential barrier was also observed for single kinked SnO₂ NW [44] and for Zn₂GeO₄ NW networks [48]. The improved rapidity can be attributed to a diminishing of the influence of surface effects (adsorption/photodesorption of oxygen molecules) which are rela-

tively slow processes [5,48] and to an increased role of the potential barrier, whose height modulation at UV illumination is relatively much faster [44,48,50].

In the case of exposure to ethanol molecules of Device 2 the decrease in barrier height occurs due to a release of electron after oxidation of the ethanol molecules (see Fig. 7(a,b)) [5,39]:



The enhanced sensing properties of Device 3 based on Fe-doped ZnO-T alloyed with Fe₂O₃ micro- and nanoparticles have a different origin than in the case of Device 2. In this case the presence of Fe₂O₃ plays the dominant role [51–53]. We consider that the

Table 2
Parameters of ethanol vapour sensors based on single semiconducting oxide nanostructures.

Sensing material	EtOH conc. (ppm)	R_{air}/R_{gasor} I_{gas}/I_{air}	Operating temp. (°C)	r (s)	d (s)	Year of pub.
Single Fe ₂ O ₃ NW [65]	200	≈3.5	RT	–	–	2008
Single MoO ₃ NB [66]	100	≈1.23	100	14	25–30	2014
Single ZnO ND [67]	200	≈30	350	10	15	2013
Single Pd-ZnO MW [68]	200	≈1.15	400	–	–	2012
Single CeO ₂ NW [69]	200	≈1.3	RT	–	–	2008
Single CuO NW [70]	500	≈1.6	RT	–	–	2009
Single Pd-doped SnO ₂ NR [71]	100	1.8	230	18	28	2014
Fe-doped ZnO-T (Device 1)	100	9	RT	43.8	98	This work
Two interconnected Fe-doped ZnO-T (Device 2)	100	16.5	RT	17.9	25.6	This work
Fe-doped ZnO-T alloyed with Fe ₂ O ₃ micro- and nanoparticles (Device 3)	100	51	RT	2.5	12.3	This work

enhanced UV sensing properties are due to the formation of a type II heterojunction [19,27], which is very efficient for the separation of photogenerated electron-hole pairs and a diminishing of charge recombination and the PPC effect [54].

The ultra-fast gas detection and recovery of Device 3 can be explained by the catalytic effect of Fe₂O₃ micro- and nanoparticles which facilitates the speed of these reactions [39]. Kim et al. [55] demonstrated an increased response and recovery of ethanol vapour sensors by the functionalization of SnO₂ hollow spheres with NiO, which act as a catalyst for surface reactions. This applies especially for the recovery process due to an enhanced transfer to the surface of electrons or negatively charged adsorbed oxygen.

Fe₂O₃ is widely used as a catalyst which can catalyze the dehydrogenation reaction and the ring-opening reaction of hydro-carbons, which is beneficial for gas sensing [39], and can explain the increase in ethanol vapour response which may play a significant role in its selective detection [51–53]. Yu et al. [39] demonstrated that the ethanol vapour response of a ZnO-based sensors can be increased by Fe doping due to the adherence of Fe₂O₃ nanoparticles on the ZnO surface and oxygen vacancies. Tang et al. [56] also demonstrated that the additional Fe₂O₃ nanoparticles can promote the adsorption of gas molecules on the oxide surface and accelerate the oxidizing process. Furthermore, due to the different work functions of Fe₂O₃ and ZnO [19,27] an electron flow will take place from Fe₂O₃ to ZnO, causing a higher concentration of electrons in ZnO, i.e. more adsorbed oxygen molecules on the surface of the tetrapod, which will lead to a higher oxygen coverage and a decrease of sensor resistance, resulting in a higher gas response (see Fig. 7(c)) [39,57]. An increase in adsorbed oxygen molecules leads to a larger quantity of charge transfer, also resulting in a faster response [58].

3.7. DFT study of H₂, CO, ethanol and CH₄ gas molecule interactions on Fe₂O₃ doped ZnO(0001) surface

Our recent DFT calculations of the Fe₂O₃ doped ZnO(0001) surface reveal that Fe dopant atoms prefer to be in the top surface layer, replacing 3 Zn with 2 Fe atoms [27]. While a CH₄ molecule shows a weak interaction with this doped surface, exhibiting only physisorption, the H₂, CO and ethanol molecules have been found to interact strongly with the surface [27]. We have further analysed the interaction of these molecule with the Fe₂O₃:ZnO(0001) surface in order to quantify the gas molecule sensing mechanism.

The H₂ gas molecule is found to interact strongly with the surface with a release of 308.8 kJ/mol energy [27]. The hydrogen atoms lose electrons to become positively charged (0.535(H_a) and 0.132 e⁻ (H_b)) atoms, and connect with one of the surface oxygen (O) to form a water molecule, which becomes slightly more negatively charged compared to other surface O atoms. The charge density difference plot (Fig. 8(a)) shows excess negative charge densities on the Fe dopant atoms, indicating charge re-distribution on the

surface and interactions with the molecule, where a Fe atom (Fe1) close to the molecule loses 0.50 e⁻ charge. A comparison of the Bader charges of the bare Fe₂O₃:ZnO(001) surface and atoms of the isolated gas phase molecule with that of the system in the adsorbed geometry is presented in Table S4.

The CO molecule is found to connect to a surface oxygen atom, forming a bent CO₂ geometry on the surface, with a release of -196.9 kJ/mol energy [27]. **Bader** charge calculations show that the C atom becomes more positively charged (1.63 e⁻), transfer-ring 0.13 e⁻ charge to the bound surface oxygen (O2). We note an excess negative charge on the surface oxygen atom bonded to the CO molecule and also on Fe atoms, indicating Fe-O and Fe-C interactions (Fig. 8(b)).

The ethanol molecule binds to the Fe dopant atom, through O-Fe and H-O bonds, releasing -143.5 kJ/mol energy [27]. The charge density difference plot (Fig. 8(c)) shows that charge transfer occurs between the surface oxygen (O_{SUF}) and H atom of the molecule (H1) and between the oxygen atom of the molecule (O) and the surface Fe atom (Fe2), where the Fe2 atom loses 0.13 e⁻. The hydrogen atom (H1) becomes less positively charged by losing 0.09 e⁻ charge, while the O atom bonded with the surface Fe atom, loses 0.02 e⁻ charge.

Compared to other gas molecules investigated in the present study, the CH₄ gas molecule is found to bind weakly with the Fe₂O₃:ZnO(0001) surface, with a binding energy of only -28.6 kJ/mol [27]. **Bader** charge analysis shows that the carbon (C) and the hydrogen atom nearest the surface (H1) gain and lose ~0.1 e⁻, respectively (Fig. 8(d)).

A comparison of the Bader charges of atoms in the adsorbed geometry with those of the isolated gas phase molecule and bare Fe₂O₃:ZnO(0001) surface is presented in Table S4. Our results indicate that Fe doping affects the sensing of different gas molecules, exhibiting significant charge transfer between the gas molecule and the surface. These findings are similar to the H₂ gas molecule sensing mechanism on Zn-doped copper oxides [29].

4. Conclusions

In this work a new step towards the development of bottom-up nanotechnologies was reported. We have fabricated, for the first time devices based on a single or two interconnected ZnO tetrapods doped with Fe and alloyed with Fe₂O₃ micro- and nanoparticles. The improved sensing properties towards UV detection and ethanol vapour sensing of three types of devices are investigated. Device 1 based on a single Fe-doped ZnO tetrapod demonstrated improved UV sensing response and rapidity compared to previously reported pristine ZnO-T, revealing the importance of doping microstructures with semiconducting oxides. An on/off ratio of 18 at an applied bias voltage of 1 V was obtained for Device 1 under UV illumination.

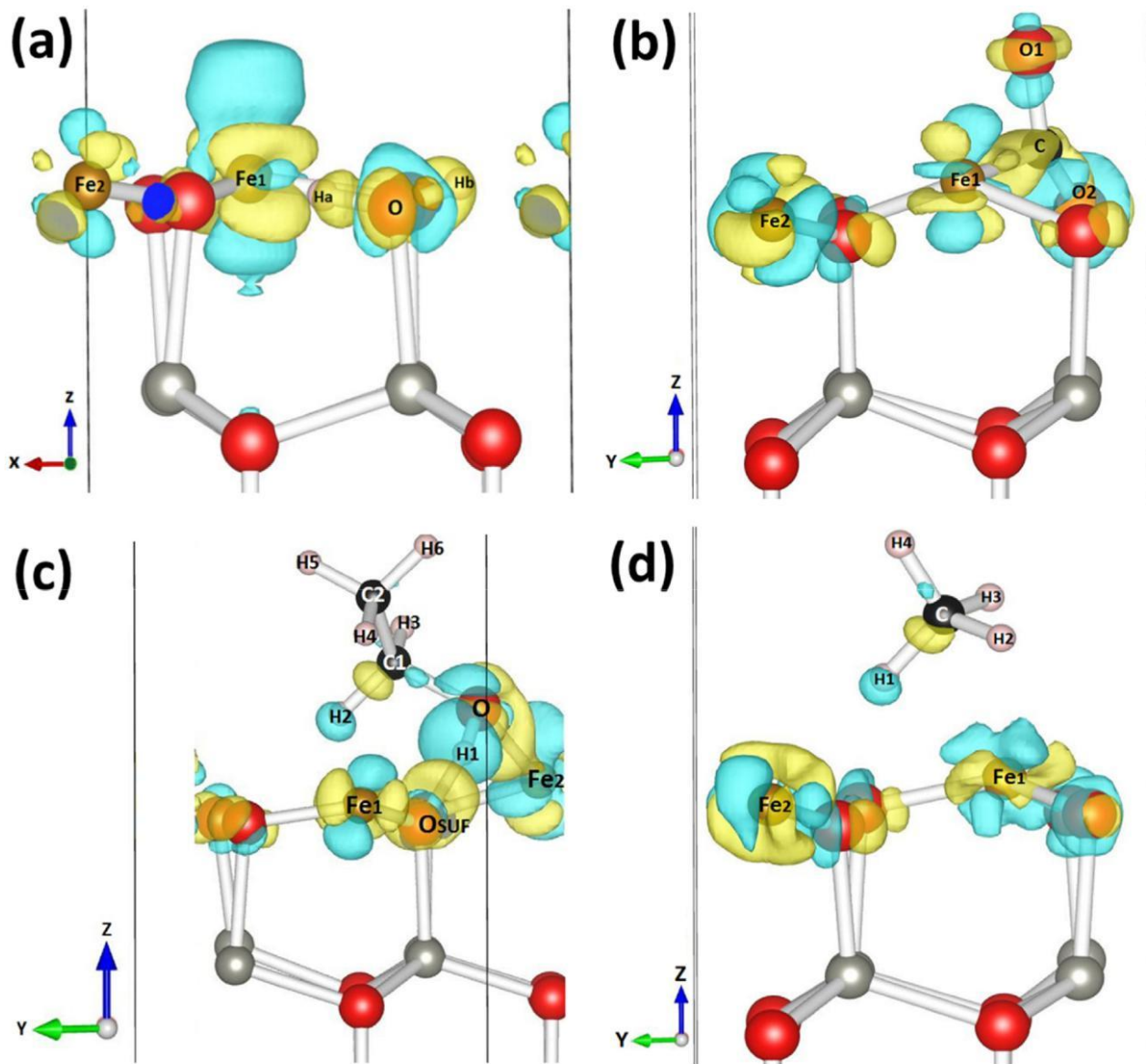


Fig. 8. (a) Electronic density difference plot of the: (a) H₂; (b) CO; (c) ethanol; and (d) CH₄ gas molecules on the Fe₂O₃ :ZnO(0001) surface, showing charge transfer in the regions between the molecule and the surface atoms upon interaction. Blue contours indicate electron density increases by 0.02 electrons/Å³ and yellow contours indicate electron density decreases by 0.02 electrons/Å³. (For interpretation of the references to colour in this figure legend, the reader is referred to the web version of this article.)

Improved gas sensing properties with good selectivity to ethanol vapour were also observed by doping with Fe in ZnO tetrapods.

Device 2 based on two interconnected Fe-doped ZnO tetrapods demonstrated a further improvement in UV sensing properties, namely an on/off ratio of 54 at applied bias voltage of 1 V and faster recovery times, which is very important for optical communications. For example at 1 V applied bias voltage the slow time component of the recovery curve (τ_2) for Device 2 is 4.53 s compared with 39.4 s for Device 1. In the gas sensing investigations, no changes in selectivity were observed compared to Device 1, only improvements in the rapidity and gas response. This reveals that an additional potential barrier created at the interface of two tetrapods does not have an impact on the selectivity.

In Device 3, based on a Fe-doped ZnO tetrapod alloyed with Fe₂O₃ NPs and MPs, an exceptional improvement in performance was observed. The UV response increased by about 80 times compared to Device 1 (on/off ratio from 18 to 1390). Besides the increase in response, an increase in recovery time was observed as well

($\tau_2 = 8.7$ s at 1 V applied bias voltage), but even more interesting results were obtained in the gas sensing investigations. Increases in ethanol vapour response were observed from 9 and 16.5 for Devices 1 and 2, respectively, to 51 for Device 3. Another important factor is the reduced dependence of the gas sensing properties of Device 3 on the RH, which was attributed to the presence of Fe₂O₃ NPs and MPs, which act as good adsorbers for water molecules and thus prevent their competitive interaction with the Fe-doped ZnO-T surface.

Acknowledgements

Dr. Lupan acknowledges the Alexander von Humboldt Foundation for the research fellowship for experienced researchers 3-3MOL/1148833 STP at the Institute for Materials Science, University of Kiel, Germany. Dr. Mishra acknowledges SEED money support from University of Petroleum and Energy Studies (UPES), Dehradun, India. Further funding is acknowledged for the project A5 in CRC 1261 from the German Research Foundation (DFG).

This research was partly supported by the project Institutional 45inst-15.817.02.29A funded by the Government of the Republic of Moldova .

References

- [1] O. Lupan, L. Chow, T. Pauporté, L.K. Ono, B. Roldan Cuenya, G. Chai, Highly sensitive and selective hydrogen single-nanowire nanosensor, *Sens. Actuators B* 173 (2012) 772–780.
- [2] O. Lupan, L. Chow, G. Chai, A single ZnO tetrapod-based sensor, *Sens. Actuators B* 141 (2009) 511–517.
- [3] H.-R. Kim, A. Haensch, I.-D. Kim, N. Barsan, U. Weimar, J.-H. Lee, The role of NiO doping in reducing the impact of humidity on the performance of SnO₂-based gas sensors: synthesis strategies, and phenomenological and spectroscopic studies, *Adv. Funct. Mater.* 21 (2011) 4456–4463.
- [4] D.P. Volanti, A.A. Felix, M.O. Orlandi, G. Whitfield, D.J. Yang, E. Longo, H.L. Tuller, J.A. Varela, The role of hierarchical morphologies in the superior gas sensing performance of CuO-based chemiresistors, *Adv. Funct. Mater.* 23 (2013) 1759–1766.
- [5] V. Postica, I. Hölken, V. Schneider, V. Kaidas, O. Polonskyi, V. Cretu, I. Tiginyanu, F. Faupel, R. Adelung, O. Lupan, Multifunctional device based on ZnO: Fe nanostructured films with enhanced UV and ultra-fast ethanol vapour sensing, *Mater. Sci. Semicond. Process.* 49 (2016) 20–33.
- [6] N. Yamazoe, New approaches for improving semiconductor gas sensors, *Sens. Actuators B* 5 (1991) 7–19.
- [7] C.S. Lao, M.-C. Park, Q. Kuang, Y. Deng, A.K. Sood, D.L. Polla, Z.L. Wang, Giant enhancement in UV response of ZnO nanobelts by polymer surface-functionalization, *J. Am. Chem. Soc.* 129 (2007) 12096–12097.
- [8] J.-H. Kim, A. Katoch, S.S. Kim, Optimum shell thickness and underlying sensing mechanism in p–n CuO–ZnO Core–Shell nanowires, *Sens. Actuators B* 222 (2016) 249–256.
- [9] A. Kolmakov, D.O. Klenov, Y. Lilach, S. Stemmer, M. Moskovits, Enhanced gas sensing by individual SnO₂ nanowires and nanobelts functionalized with Pd catalyst particles, *Nano Lett.* 5 (2005) 667–673.
- [10] C.L. Zhu, Y.J. Chen, R.X. Wang, L.J. Wang, M.S. Cao, X.L. Shi, Synthesis and enhanced ethanol sensing properties of -Fe₂O₃/ZnO heteronanostructures, *Sens. Actuators B* 140 (2009) 185–189.
- [11] S. Si, C. Li, X. Wang, Q. Peng, Y. Li, Fe₂O₃/ZnO core-shell nanorods for gas sensors, *Sens. Actuators B* 119 (2006) 52–56.
- [12] L. Huang, H. Fan, Room-temperature solid state synthesis of ZnO/-Fe₂O₃ hierarchical nanostructures and their enhanced gas-sensing properties, *Sens. Actuators B* 171–172 (2012) 1257–1263.
- [13] D. Zhu, Y. Fu, W. Zang, Y. Zhao, L. Xing, X. Xue, Room-temperature self-powered ethanol sensor based on the piezo-surface coupling effect of heterostructured -Fe₂O₃/ZnO nanowires, *Mater. Lett.* 166 (2016) 288–291.
- [14] D.N. Suryawanshi, D.R. Patil, L.A. Patil, Fe₂O₃-activated Cr₂O₃ thick films as temperature dependent gas sensors, *Sens. Actuators B* 134 (2008) 579–584.
- [15] S. Kim, S. Park, G.-J. Sun, S.K. Hyun, K.-K. Kim, C. Lee, Enhanced acetone gas sensing performance of the multiple-networked Fe₂O₃-functionalized In₂O₃ nanowire sensor, *Curr. Appl. Phys.* 15 (2015) 947–952.
- [16] K.S. Choi, S. Park, S.-P. Chang, Enhanced ethanol sensing properties based on SnO₂ nanowires coated with Fe₂O₃ nanoparticles, *Sens. Actuators B* 238 (2017) 871–879.
- [17] S. Minicò, S. Scirè, C. Crisafulli, R. Maggiore, S. Galvagno, Catalytic combustion of volatile organic compounds on gold/iron oxide catalysts, *Appl. Catal. B* 28 (2000) 245–251.
- [18] V. V. Kovalenko, M.N. Romyantseva, A.M. Gaskov, E.V. Makshina, V.V. Yushchenko, I.I. Ivanova, A. Ponzoni, G. Faglia, E. Comini, SnO₂/Fe₂O₃ nanocomposites: ethanol-sensing performance and catalytic activity for oxidation of ethanol, *Inorg. Mater.* 42 (2006) 1088–1093.
- [19] W. Wu, S. Zhang, X. Xiao, J. Zhou, F. Ren, L. Sun, C. Jiang, Controllable synthesis, magnetic properties, and enhanced photocatalytic activity of spindle-like mesoporous -Fe₂O₃/ZnO core-shell heterostructures, *ACS Appl. Mater. Interfaces* 4 (2012) 3602–3609.
- [20] O. Lupan, G. Chai, L. Chow, Novel hydrogen gas sensor based on single ZnO nanorod, *Microelectron. Eng.* 85 (2008) 2220–2225.
- [21] K.H. Zheng, Y.C. Zhao, K. Deng, Z. Liu, L.F. Sun, Z.X. Zhang, L. Song, H.F. Yang, C.Z. Gu, S.S. Xie, Effectively enhanced oxygen sensitivity of individual ZnO tetrapod sensor by water preadsorption, *Appl. Phys. Lett.* 92 (2008) 213116.
- [22] Z. Zhang, L. Sun, Y. Zhao, Z. Liu, D. Liu, L. Cao, B. Zou, W. Zhou, C. Gu, S. Xie, ZnO tetrapods designed as multiterminal sensors to distinguish false responses and increase sensitivity, *Nano Lett.* 8 (2008) 652–655.
- [23] Y. Hu, J. Zhou, P.-H. Yeh, Z. Li, T.-Y. Wei, Z.L. Wang, Supersensitive, fast-response nanowire sensors by using Schottky contacts, *Adv. Mater.* 22 (2010) 3327–3332.
- [24] F. Hernandez-Ramirez, J.D. Prades, R. Jimenez-Diaz, T. Fischer, A. Romano-Rodriguez, S. Mathur, J.R. Morante, On the role of individual metal oxide nanowires in the scaling down of chemical sensors, *Phys. Chem. Chem. Phys.* 11 (2009) 7105–7110.
- [25] J.D. Prades, R. Jimenez-Diaz, F. Hernandez-Ramirez, S. Barth, A. Cirera, A. Romano-Rodriguez, S. Mathur, J.R. Morante, Ultralow power consumption gas sensors based on self-heated individual nanowires, *Appl. Phys. Lett.* 93 (2008) 123110.
- [26] Q. Kuang, C.-S. Lao, Z. Li, Y.-Z. Liu, Z.-X. Xie, L.-S. Zheng, Z.L. Wang, Enhancing the photon- and gas-sensing properties of a single SnO₂ nanowire based nanodevice by nanoparticle surface functionalization, *J. Phys. Chem. C* 112 (2008) 11539–11544.
- [27] O. Lupan, V. Postica, J. Gröttrup, A.K. Mishra, N.H. De Leeuw, C.J.F.C. J. Rodrigues, N. Ben Sedrine, M.R. Correia, T. Monteiro, V. Cretu, I. Tiginyanu, D. Smazna, Y.K. Mishra, R. Adelung, Hybridization of zinc oxide tetrapods for selective gas sensing applications, *ACS Appl. Mater. Interfaces* (2017), <http://dx.doi.org/10.1021/acsmi.6b11337>.
- [28] J. Gröttrup, I. Paulowicz, A. Schuchardt, V. Kaidas, S. Kaps, O. Lupan, R. Adelung, Y.K. Mishra, Three-dimensional flexible ceramics based on interconnected network of highly porous pure and metal alloyed ZnO tetrapods, *Ceram. Int.* 42 (2016) 8664–8676.
- [29] V. Cretu, V. Postica, A.K. Mishra, M. Hoppe, I. Tiginyanu, Y.K. Mishra, L. Chow, N.H. de Leeuw, R. Adelung, O. Lupan, Synthesis, characterization and DFT studies of zinc-doped copper oxide nanocrystals for gas sensing applications, *J. Mater. Chem. A* 4 (2016) 6527–6539.
- [30] K. Xu, Z. Wang, F. Wang, Y. Huang, F. Wang, L. Yin, C. Jiang, J. He, Ultrasensitive phototransistors based on few-layered HfS₂, *Adv. Mater.* 27 (2015) 7881–7887.
- [31] G. Kresse, J. Hafner, Ab initio molecular dynamics for liquid metals, *Phys. Rev. B* 47 (1993) 558.
- [32] G. Kresse, J. Hafner, Ab initio molecular-dynamics simulation of the liquid-metal–amorphous-semiconductor transition in germanium, *Phys. Rev. B* 49 (1994) 14251.
- [33] P.E. Blöchl, O. Jepsen, O.K. Andersen, Improved tetrahedron method for Brillouin-zone integrations, *Phys. Rev. B* 49 (1994) 16223–16233.
- [34] S. Grimme, Semiempirical GGA-type density functional constructed with a long-range dispersion correction, *J. Comput. Chem.* 27 (2006) 1787–1799.
- [35] R.F.W. Bader, *Atoms in Molecules*, Wiley Online Library, 1990.
- [36] G.W. Watson, E.T. Kelsey, N.H. de Leeuw, D.J. Harris, S.C. Parker, Atomistic simulation of dislocations, surfaces and interfaces in MgO, *J. Chem. Soc. Faraday Trans. 92* (1996) 433–438.
- [37] H.J. Monkhorst, J.D. Pack, Special points for Brillouin-zone integrations, *Phys. Rev. B* 13 (1976) 5188.
- [38] Z.L. Wang, J. Song, Piezoelectric nanogenerators based on zinc oxide nanowire arrays, *Science* 312 (2006) 242–246.
- [39] A. Yu, J. Qian, H. Pan, Y. Cui, M. Xu, L. Tu, Q. Chai, X. Zhou, Micro-lotus constructed by Fe-doped ZnO hierarchically porous nanosheets: preparation, characterization and gas sensing property, *Sens. Actuators B* 158 (2011) 9–16.
- [40] D. Gedamu, I. Paulowicz, S. Kaps, O. Lupan, S. Wille, G. Haidarschin, Y.K. Mishra, R. Adelung, Rapid fabrication technique for interpenetrated ZnO nanotetrapod networks for fast UV sensors, *Adv. Mater.* 26 (2014) 1541–1550.
- [41] O. Lupan, V. Cretu, V. Postica, M. Ahmadi, B.R. Cuenya, L. Chow, I. Tiginyanu, B. Viana, T. Pauporté, R. Adelung, Silver-doped zinc oxide single nanowire multifunctional nanosensor with a significant enhancement in response, *Sens. Actuators B* 223 (2016) 893–903.
- [42] J.D. Prades, F. Hernandez-Ramirez, R. Jimenez-Diaz, M. Manzanara, T. Andreu, A. Cirera, A. Romano-Rodriguez, J.R. Morante, The effects of electron-hole separation on the photoconductivity of individual metal oxide nanowires, *Nanotechnol* 19 (2008) 465501.
- [43] C. Soci, A. Zhang, B. Xiang, S.A. Dayeh, D.P.R. Aplin, J. Park, X.Y. Bao, Y.H. Lo, D. Wang, ZnO nanowire UV photodetectors with high internal gain, *Nano Lett.* 7 (2007) 1003–1009.
- [44] L. Gan, M. Liao, H. Li, Y. Ma, T. Zhai, Geometry-induced high performance ultraviolet photodetectors in kinked SnO₂ nanowires, *J. Mater. Chem. C* 3 (2015) 8300–8306.
- [45] M. Thepnurat, T. Chairuangri, N. Hongsith, P. Ruankham, S. Choopun, Realization of interlinked ZnO tetrapod networks for UV sensor and room-temperature gas sensor, *ACS Appl. Mater. Interfaces* 7 (2015) 24177–24184.
- [46] W.-P. Tai, J.-H. Oh, Humidity sensing behaviors of nanocrystalline Al-doped ZnO thin films prepared by sol–gel process, *J. Mater. Sci. Mater. Electron.* 13 (2002) 391–394.
- [47] P.V. Adhyapak, U.P. Mulik, D.P. Amalnerkar, I.S. Mulla, Low temperature synthesis of needle-like -FeOOH and their conversion into -Fe₂O₃ nanorods for humidity sensing application, *J. Am. Ceram. Soc.* 96 (2013) 731–735.
- [48] C. Yan, N. Singh, P.S. Lee, Wide-bandgap Zn₂GeO₄ nanowire networks as efficient ultraviolet photodetectors with fast response and recovery time, *Appl. Phys. Lett.* 96 (2010) 053108.
- [49] A. Gurlo, Interplay between O₂ and SnO₂: oxygen ionosorption and spectroscopic evidence for adsorbed oxygen, *ChemPhysChem* 7 (2006) 2041–2052.
- [50] S.-M. Peng, Y.-K. Su, L.-W. Ji, C.-Z. Wu, W.-B. Cheng, W.-C. Chao, ZnO nanobridge array UV photodetectors, *J. Phys. Chem. C* 114 (2010) 3204–3208.
- [51] H. Tang, M. Yan, H. Zhang, S. Li, X. Ma, M. Wang, D. Yang, A selective NH₃ gas sensor based on Fe₂O₃-ZnO nanocomposites at room temperature, *Sens. Actuators B* 114 (2006) 910–915.

- [52] M. Ivanovskaya, D. Kotsikau, G. Faglia, P. Nelli, S. Irkaev, Gas-sensitive properties of thin film heterojunction structures based on Fe₂O₃-In₂O₃ nanocomposites, *Sens. Actuators B* 93 (2003) 422–430.
- [53] M. Ivanovskaya, D. Kotsikau, G. Faglia, P. Nelli, Influence of chemical composition and structural factors of Fe₂O₃/In₂O₃ sensors on their selectivity and sensitivity to ethanol, *Sens. Actuators B* 96 (2003) 498–503.
- [54] H. Zhou, Y. Qu, T. Zeid, X. Duan, Towards highly efficient photocatalysts using semiconductor nanoarchitectures, *Energy Environ. Sci.* 5 (2012) 6732–6743.
- [55] H.-R. Kim, K.-I. Choi, K.-M. Kim, I.-D. Kim, G. Cao, J.-H. Lee, Ultra-fast responding and recovering C₂H₅OH sensors using SnO₂ hollow spheres prepared and activated by Ni templates, *Chem. Commun.* 46 (2010) 5061–5063.
- [56] H. Tang, M. Yan, H. Zhang, S. Li, X. Ma, M. Wang, D. Yang, A selective NH₃ gas sensor based on Fe₂O₃-ZnO nanocomposites at room temperature, *Sens. Actuators B* 114 (2006) 910–915.
- [57] L. Li, Z. Du, T. Wang, Enhanced sensing properties of defect-controlled ZnO nanotetrapods arising from aluminum doping, *Sens. Actuators B* 147 (2010) 165–169.
- [58] W. Li, S. Ma, Y. Li, G. Yang, Y. Mao, J. Luo, D. Gengzang, X. Xu, S. Yan, Enhanced ethanol sensing performance of hollow ZnO/SnO₂ core-shell nanofibers, *Sens. Actuators B* 211 (2015) 392–402.
- [59] G.Y. Chai, L. Chow, O. Lupan, E. Rusu, G.I. Stratan, H. Heinrich, V.V. Ursaki, I.M. Tiginyanu, Fabrication and characterization of an individual ZnO microwire-based UV photodetector, *Solid State Sci.* 13 (2011) 1205–1210.
- [60] W.Y. Weng, S.J. Chang, C.L. Hsu, T.J. Hsueh, A ZnO-Nanowire phototransistor prepared on glass substrates, *ACS Appl. Mater. Interfaces* 3 (2011) 162–166.
- [61] G. Cheng, X. Wu, B. Liu, B. Li, X. Zhang, Z. Du, ZnO nanowire Schottky barrier ultraviolet photodetector with high sensitivity and fast recovery speed, *Appl. Phys. Lett.* 99 (2011) 203105.
- [62] J. Dai, C. Xu, X. Xu, J. Guo, J. Li, G. Zhu, Y. Lin, Single ZnO microrod ultraviolet photodetector with high photocurrent gain, *ACS Appl. Mater. Interfaces* 5 (2013) 9344–9348.
- [63] H. Ding, J. Shao, Y. Ding, W. Liu, H. Tian, X. Li, One-dimensional Au-ZnO heteronanostructures for ultraviolet light detectors by a two-step dielectrophoretic assembly method, *ACS Appl. Mater. Interfaces* 7 (2015) 12713–12718.
- [64] O. Lupan, T. Braniste, M. Deng, L. Ghimpu, I. Paulowicz, Y.K. Mishra, L. Kienle, R. Adelung, I. Tiginyanu, Rapid switching and ultra-responsive nanosensors based on individual shell-core Ga₂O₃/Ga_N:O_x@SnO₂ nanobelt with nanocrystalline shell in mixed phases, *Sens. Actuators B* 221 (2015) 544–555.
- [65] L. Liao, Z. Zheng, B. Yan, J.X. Zhang, H. Gong, J.C. Li, C. Liu, Z.X. Shen, T. Yu, Morphology controllable synthesis of -Fe₂O₃ 1D nanostructures: growth mechanism and nanodevice based on single nanowire, *J. Phys. Chem. C* 112 (2008) 10784–10788.
- [66] O. Lupan, V. Cretu, M. Deng, D. Gedamu, I. Paulowicz, S. Kaps, Y.K. Mishra, O. Polonskyi, C. Zamponi, L. Kienle, V. Trofim, I. Tiginyanu, R. Adelung, Versatile growth of freestanding orthorhombic -molybdenum trioxide nano- and microstructures by rapid thermal processing for gas nanosensors, *J. Phys. Chem. C* 118 (2014) 15068–15078.
- [67] M.R. Alenezi, A.S. Alshammari, K.D.G.I. Jayawardena, M.J. Beliatas, S.J. Henley, S.R.P. Silva, Role of the exposed polar facets in the performance of thermally and UV activated ZnO nanostructured gas sensors, *J. Phys. Chem. C* 117 (2013) 17850–17858.
- [68] G.Y. Chai, O. Lupan, E.V. Rusu, G.I. Stratan, V.V. Ursaki, V. S. ontea, H. Khallaf, L. Chow, Functionalized individual ZnO microwire for natural gas detection, *Sens. Actuators A* 176 (2012) 64–71.
- [69] L. Liao, H.X. Mai, Q. Yuan, H.B. Lu, J.C. Li, C. Liu, C.H. Yan, Z.X. Shen, T. Yu, Single CeO₂ nanowire gas sensor supported with Pt nanocrystals: gas sensitivity, surface bond states, and chemical mechanism, *J. Phys. Chem. C* 112 (2008) 9061–9065.
- [70] L. Liao, Z. Zhang, B. Yan, Z. Zheng, Q.L. Bao, T. Wu, C.M. Li, Z.X. Shen, J.X. Zhang, H. Gong, Multifunctional CuO nanowire devices: p-type field effect transistors and CO gas sensors, *Nanotechnology* 20 (2009) 085203.
- [71] J. Ma, Y. Liu, H. Zhang, P. Ai, N. Gong, Y. Zhang, Synthesis and high sensing properties of a single Pd-doped SnO₂ nanoribbon, *Nanoscale Res. Lett.* 9 (2014) 1–10.

Biographies



Lupan Oleg is a fellow for experienced researchers supported by Alexander von Humboldt Foundation at Christian-Albrechts Universität zu Kiel (CAU), Kiel University, Germany, in the research group “Functional Nanomaterials” of Professor Adelung, Germany. He received his M.S. in microelectronics and semiconductor devices from the Technical University of Moldova (TUM) in 1993. He received his Ph.D. from the Institute of Applied Physics, Academy of Sciences of Moldova (ASM) in 2005. His post-doctorate research activities were carried out at the French CNRS, Paris, France and the University of Central Florida, USA. He received his doctor habilitate degree (Dr. Eng.) in solid state electronics, microelectronics and

nanoelectronics from the Institute of Electronic Engineering and Nanotechnologies

of ASM in 2011. His post-habilitation activities were performed at the University of Paris-IRCP-ENSCP-CNRS, Paris, France and the Institute for Materials Science, University of Kiel, CAU, Germany. He is an Associate Professor and research scientist in solid state electronics and nanoelectronics at TUM. He started a new research group “Nanotechnologies for sensing nanodevices” at TUM in 2015. His current research interests include sensors, nanosensors, optoelectronic devices, nanotechnologies and nanodevices. E-mail: lupanoleg@yahoo.com or llu@tf.uni-kiel.de.



Postica Vasile is at present a Ph. D. candidate in the group of Nanotechnologies for sensing nanodevices of Professor Lupan, TUM, Moldova. He studied microelectronics and nanotechnologies at the TUM and received his Engineer-ing degree diploma (ranked as the best one at TUM by the TUM Senate) in 2014 working on the synthesis of zinc oxide-copper oxide composite and its surface modification. He continued for master thesis in Nanotechnologies at Technical University of Moldova (ranked as TOP1 in 2016 at TUM by the TUM Senate). He received his M.Sc. in microelectronics and nanotechnologies from the Technical University of Moldova in 2016. His current research interests are nanostructuring of semiconducting oxides,

thin films and nanowires, gas sensors, nanosensors and UV photodetectors’ development.



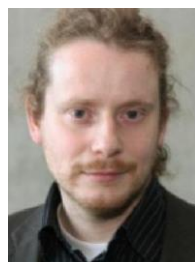
Jorit Gröttrup is currently working as a Ph. D. candidate in the Functional Nanomaterials Group of Professor Adelung, Christian-Albrechts-Universität zu Kiel (CAU), Germany. He studied Materials Science & Engineering at the CAU and received his B.Sc. in 2011 working on the synthesis of zinc oxide needles by vapour liquid solid process and flame transport method. In 2013 he finished his M.Sc. at the CAU on the synthesis and characterization of three dimensional interconnected zinc oxide networks. His current research interests include nano- and microstructured networks of semiconducting oxides, highly-porous three dimensional carbon materials and piezotronic magneto-electric sensors.



Abhishek Kumar Mishra is working as an Assistant Professor at University of Petroleum and Energy Studies, Dehradun, India. He is Computational Material Scientist and prior joining UPES, worked for 3.5 years at University College London, London on ESPRC (UK) grant for Designing Novel Materials for CO₂ Capture and Conversion. After completing Ph.D. in 2008 from University of Luc-know, India in Physics, he worked at various international and national universities, including postdoc positions at Texas A&M University, TX, USA; Banaras Hindu University, Varanasi, JNCASR, Bangalore. His research expertise is in modeling and simulations of materials using first-principles based techniques.



Nora de Leeuw is a prominent scientist with an international reputation in the field of computational chemistry of materials and minerals. Specific research interests include the development of models to study biocompatible materials for tissue engineering applications, and the computer-aided design of sustainable catalysts for the conversion of carbon dioxide to fuels and chemicals under mild reaction conditions. She has been awarded research fellowships by the EPSRC and Royal Society and holds pro-fessorial appointments at Cardiff University and Utrecht University, as well as an AWE William Penney fellowship at University College London.



Ainer Adelung is full professor and Chairholder of the Functional Nanomaterials group established in 2007 at the Institute for Materials Science, University of Kiel, Germany. He received his Ph.D. (rer. nat) in Physics in 2000 from Institute of Experimental and Applied Physics, University of Kiel and during 2001–2002 he was at Case Western Reserve University in Cleveland (USA) as Feodor Lynen (Alexander von Humboldt) Research Fellow. In 2006 he finished his Habilitation at Institute for Materials Science in Kiel and then continued as Heisenberg Professor (DFG grant). Main research interests are the growth, understanding and utilization of metal oxides and porous materials.